2184 Vol. 61, No. 9 / 20 March 2022 / Applied Optics Research Article

applied optics

# Visible light waveband Dammann grating based on all-dielectric metasurface

基于全电介质超表面的可见光波段达曼光栅

**Xiaoran Zheng,[1] Jiaqi Yang,[2] Runqiu Wang,[1] and Tian Lan[1,*]**

[1]Key Laboratory of Photoelectric Imaging Technology and System, Ministry of Education of China, School of Optics and Photonics, Beijing Institute of Technology, Beijing, 100081, China
[2]Department of Physics and Mathematics, University of Eastern Finland, Joensuu, 80100, Finland
*Corresponding author: lantian@bit.edu.cn

Received 11 November 2021; revised 29 January 2022; accepted 5 February 2022; posted 7 February 2022; published 14 March 2022

背景

达曼光栅可以生成特定排列中的斑点阵列

方案及结果
基于全电介质超表面的达曼光栅，可以产生一个5*5衍射角为20°*20°的衍射点阵列，工作波段为650~690nm，效率≥60%，对比度≤0.33

展望

**Dammann gratings (DGs) can generate a spot array in a particular arrangement. In recent years, DGs have been used in many fields such as laser beam splitting and optical coupling. Nanograting encoding technology can achieve a high signal-to-noise ratio and high-efficiency diffraction distribution; it also provides new design ideas for realizing the miniaturization and deviceization of DGs. In this work, we have comprehensively studied the DG based on an all-dielectric metasurface, which can produce a $5 \times 5$ diffraction spot array with a diffraction angle of $20^\circ \times 20^\circ$. In an operation waveband from 650 to 690 nm, the DG has superior performance with high efficiency $\geq 60\%$; meanwhile, it achieves a relative low contrast ratio $\leq 0.33$. Owing to high efficiency, wide waveband performance, and polarization insensitive property, the all-dielectric metasurface DG can provide possibilities for various application, including laser technology and optical information processing.** 

https://doi.org/10.1364/AO.448192

## 1. INTRODUCTION

背景及GAP

A Dammann grating (DG) is a diffractive optical element (DOE) composed of a series of position-encoded binary phase structures, which can generate an array of spots with required intensity distribution in the far field. Due to the convenience and simplicity of DG, it greatly decreases the complexity of the optical system and allows beam splitting by DG at a lower cost. DGs have been applied to subsecond laser technology, laser detection, laser direct writing, 3D measurement, particle manipulation, optical fiber communication, and other fields due to its fascinating properties such as high diffraction efficiency, small size, and light weight [1–7]. Dammann first proposed DG in 1971. Its earliest design was a symmetrical phase structure with many transition coordinates capable of generating a spot array but in low efficiency [1]. With the rapid development of computer technology, a lot of optimization algorithms such as simulated annealing (SA) and genetic algorithms (GA) have been used to obtain the phase transition values of DG with high diffraction efficiency and good intensity uniformity [2]. Among them, Zhou used numerical optimization method to obtain the numerical solutions of 2 to 31 and $64 \times 64$ high-beam-splitting-ratio DGs [4]. In recent years, a series of new grating devices such as circular DGs, 3D DGs, and distorted DGs has been further developed [8–10].

There have been some ways to realize the DGs, such as nanoscale 3D printing [11], ferroelectric liquid crystal [12], metasurface [13–18], and so on, whose design forms are closely combined with practical applications [11–19]. The previous DG phase control methods generally depend on different etching depth in a transparent dielectric substrate. Varied etch depths allow flexible phase shifts but lack modulation accuracy. There is often a dilemma between the complexity of the manufacturing process and the excellent performance [20]. In recent years, metasurfaces have been used in the design of DGs [13–18], because of their compactness, high efficiency, and reduced fabrication complexity. A metasurface is composed of a single nanostructure layer, which can retain efficient control of the phase, polarization, and amplitude of light [21,22]. Compared with the inevitable losses in the plasmonic metasurface DOE, the all-dielectric metasurface exhibits higher efficiency and more closely integrates with the semiconductor technology in the visible and infrared (IR) bands [23,24]. The all-dielectric metasurface DGs have been proposed mainly in the near-infrared band [13,14,17]. Li *et al.* demonstrated an all-silicon nanorod-based DG for IR beam shaping, with circular polarization incident light [13]. Yang *et al.* realized a polarization-insensitive DG of a cuboid silicon nanorod array [14]. Ni *et al.* designed a metasurface for structured light projection over a field of view over 120° using the principle of DG [17]. The metasurfaces to realize laser beam splitting in the visible light band have also been proposed successively [25–28]. However, the main method for realizing the array of laser beam splitting is still DG, as a binary structure is relatively simple and flexible. The DGs of a metasurface in the visible light band are required; however, few are reported [15,16], and their efficiency needs to be improved.

方案及结论

In this paper, we demonstrate a 2D all-dielectric DG that utilized a single layer of nanopillars to maximize the local interaction between incident light and nanostructure. These $TiO_2$ nanopillars allow better control of phases of incident light and further modify the output wavefront [29]. Based on this scheme, the proposed DG can achieve $5 \times 5$ beam splitting with high efficiency and high uniformity in the far field, operating in the visible range from 650 to 690 nm. The conversion efficiency of the DG reaches $\geq 60\%$ with a contrast ratio $\leq 0.33$. The DG is not only polarization-insensitive but can also work in a wide operation bandwidth, which is significant for practical applications. Meanwhile, the DG is composed of only two different sizes of cylindrical antennas, which makes the design and manufacturing easier and flexible.

达曼光栅仅由两种不同尺寸的圆柱形天线组成，使得设计和制造更加容易和灵活。

## 2. STRUCTURE AND PRINCIPLE

达曼光栅(DG)是一种典型的二元光学元件，能够产生光斑阵列。DG的分段振幅传输系数分别为1或-1，对应相位分别为0或π。

A Dammann grating (DG) is a typical binary optical element capable of generating a spot array. The segmented amplitude transmission coefficient of DG is 1 or $-1$, and its corresponding phase is 0 or $\pi$, respectively. For a 1D DG with a grating constant $d$, the binary phase $\arg[T(x)]$ as a function of spatial position $x$ is as shown in Fig. 1(a), where $T(x)$ is the transmission function of the DG. We can observe that $\arg[T(x)]$ at transition points jumps between two independent numbers, i.e., 0 and $\pi$.

To obtain light field distribution, the Fourier transform is employed on the transmission function $T(x)$ of the DG. Such light field on the Fourier plane is equivalent to the diffraction field and can be described as Fourier series expansion. Thus, the light field distribution $A_n$ at the $n$th diffraction order can be written as [30]

$$A_n = \begin{cases} 2\sum_{k=1}^{N}(-1)^k x_k, & n = 0 \\ \frac{1}{\pi n}\sum_{k=1}^{N}(-1)^k e^{-i2\pi n x_k}, & n \neq 0 \end{cases}, \tag{1}$$

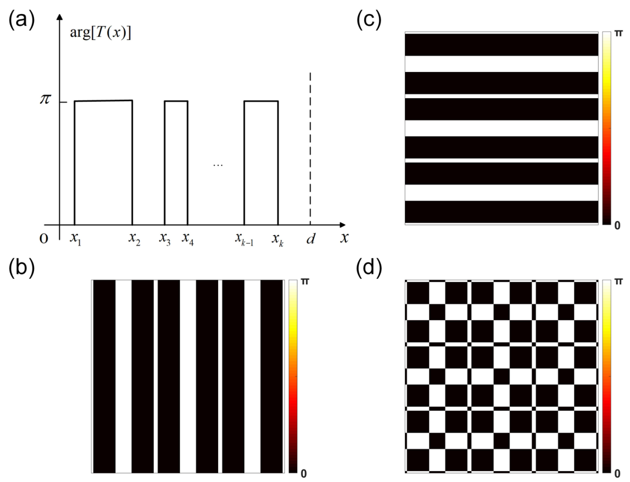


**Fig. 1.** (a) Transmittance phase function of the 1S DG changes with the spatial position within a grating constant $d$. (b) 1D Dammann phase $(0 - \pi)$ in $x$ direction. (c) 1D Dammann phase $(0 - \pi)$ in $y$ direction. (d) 2D Dammann phase, which is a superposition of the 1D DGs in (b) and (c).

where $N$ is the total number of transition points $[x_1, x_2 \ldots x_k \ldots x_N]$ within a grating constant $d$.

The intensity of the light field at diffraction order $n$ is $P_n = |A_n|^2$. As shown in Eq. (1), the diffraction field of DG is independent of grating constant $d$ and only relates to the total number of transition points $N$ and spatial coordinates $x_k$. Grating constant $d$ determines the distance between adjacent diffraction orders on the Fourier plane, which affects the beam-expansion angle. One-dimensional DG is a typical diffraction optical element for generating a linear array, and 2D DG is a kind of grating for obtaining a 2D beam array in the far-field. The superposition of two 1D DGs in orthogonal directions ($x$ and $y$), as shown in Fig. 1(b) and Fig. 1(c), forms the 2D DG in Fig. 1(d). If we consider the orthogonal DGs as $\alpha$ and $\beta$, the 2D DG [as shown in Fig. 1(d)] can be formed by logical operation and can be expressed as

一维DG是一种典型的产生线性阵列的衍射光学元件，二维DG是一种在远场中获得二维光束阵列的光栅。如图1(b)和图1(c)所示，两个正交方向(x和y)的1D DG叠加，形成图1(d)中的2D DG

$$\alpha \odot \beta = \begin{cases} \pi, & \alpha = \beta \\ 0, & \alpha \neq \beta \end{cases}. \tag{2}$$

In Eq. (2), $\alpha$ and $\beta$ are binary phase with two independent numbers, i.e., 0 and $\pi$. We can note that, when $\alpha$ is equal or unequal to $\beta$, the operation result $\alpha \odot \beta$ is $\pi$ or 0, respectively [31]. Then, we assume that the transmittance functions in the $x$ and $y$ directions are $T(x)$ and $T(y)$; following Eq. (2), the transmission function $T(x, y)$ of 2D DG can be further written as [32]

$$\arg[T(x, y)] = \arg[T(x)] \odot \arg[T(y)]. \tag{3}$$

Here, in order to evaluate the performance of the grating, we define the conversion efficiency as the ratio between the optical power of the light projected to all target diffraction orders $\sum_{i,j \in N} P_{ij}$ and the power of the incident light $P_{\text{in}}$, which can be expressed as [4]

$$\eta = \left(\sum_{i,j \in N} P_{ij}\right) \Big/ P_{\text{in}}. \tag{4}$$

Another important parameter is the intensity contrast ratio, which is also defined as

$$C = \frac{\max(I_n) - \min(I_n)}{\max(I_n) + \min(I_n)}, \tag{5}$$

where $n$ refers to the diffraction order, and $\max(I_n)$ and $\min(I_n)$ are the maximum and minimum light intensities of all the orders. The intensity contrast ratio characterizes the intensity uniformity of all target diffraction orders on the focal plane. The smaller contrast ratio $C$ is, the more uniform the light intensity distribution at all diffraction orders becomes. We also use the diffraction angle to evaluate the beam's expansion angle. The Laguerre–Gaussian beam at 660 nm is chosen as the source to simulate the far-field distribution by using angular spectrum methods [33]. The numerical solution of the coordinates of the transition points can be directly used for calculation and simulation compile [4]. Based on the above principle, we can obtain a desired $5 \times 5$ light spot array in the far field by employing a well-designed and optimized 2D DG.

光强对比度表征了焦平面上各衍射级的光强均匀性。对比度C越小，各衍射级的光强分布越均匀。

According to the grating constant $d$ for the DG design, one period of the all-dielectric metasurface DG is shown in Fig. 2(a).

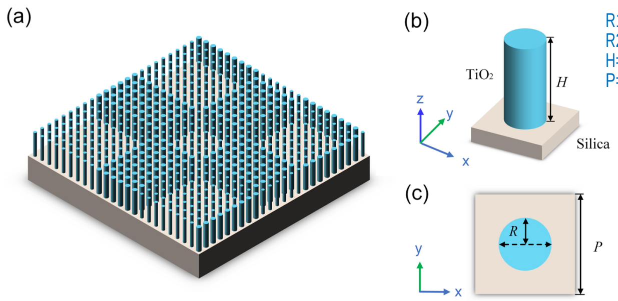


R1=82nm,
R2=121nm,
H=1300nm,
P=450nm

**Fig. 2.** (a) 2D all-dielectric metasurface DG with two sizes of $TiO_2$ cylinders $R_1 = 82$ nm and $R_2 = 121$ nm on the silica substrate. (b) Structure diagram of the unit cell with periodicity $P = 450$ nm and height $H = 1300$ nm. (c) Top view of a unit cell.

二氧化钛在可见光波段的折射率实部大，虚部小，与光波具有很强的耦合效应。因此，二氧化钛超表面可以很容易地实现整个2π的相位延迟，并实现对光波前的完全控制，并在可见光带中保持高效率.

The unit cell is a titanium dioxide ($TiO_2$) cylindrical dielectric antenna sitting on a silica substrate, as shown in Fig. 2(b). The top view of the unit cell is shown in Fig. 2(c). $TiO_2$ has a strong coupling effect with light waves due to its large real part and small imaginary part of refractive index in the visible light band. Therefore, the $TiO_2$ metasurface can easily realize a phase delay of a whole $2\pi$ and achieve complete control of the light wavefront maintaining high efficiency in the visible light band [21]. Dielectric antennas have the same height $H$ but different radii $R$. Each cylindrical antenna can be regarded as a waveguide with both sides cut off. More specifically, it can be regarded as a low-quality-factor Fabry–Perot (FP) resonator. When light is normally incident on the structure, it is mainly confined in cylindrical antennas with a high refractive index. Each antenna brings different phase shift due to different radius and consequently changes the phase distribution of the transmitted light wavefront.

Our isotropic cylindrical dielectric antenna has a unique fourfold rotational symmetry. Compared with the metasurface elements of PB phase that rely on circular polarization incident light, ours can achieve effective phase control for incident light of an arbitrary polarization state [22,34,35] and the range of optical properties of a nanopillar can be tailored by its size to expand the phase control of incident light [29]. The relationship between the radius of the antenna and the phase shift is shown by the blue line in Fig. 3(a) using finite difference time domain (FDTD) simulation software (Lumerical Inc.). In the simulation, the background refractive index of the environment is 1, and the refractive indices of the $TiO_2$ and silica in the visible light band come from the *Palik Optics Manual*. The $x$-polarization ($x$-pol) linear light at 660 nm is normally incident on the DG. The polarization state of the transmitted light will not change, but an additional phase shift will be added. When the radius of the cylindrical antenna changes from 50 to 150 nm, more than $2\pi$ phase change can be achieved. The unit cell periodicity $P$ is 450 nm, and the height $H$ is 1300 nm. The transmission coefficient of the DG maintains higher than 96% in the entire radius interval as shown by the red line in Fig. 3(a), except for the radius of 134 nm, which should be avoided. In order to obtain the phase difference of $\pi$, two typical cylinders with radii as $R_1 = 82$ nm and $R_2 = 121$ nm are chosen, as shown by the black dotted line in Fig. 3(a). It is observed that the two cylinders achieve a constant phase difference of $\pi$, and the transmission coefficient of the two cylinders is as high as

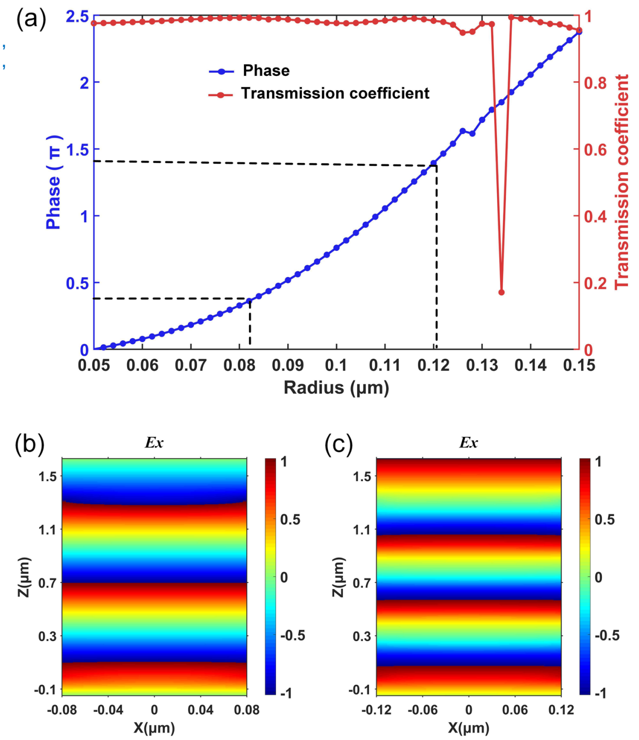


为了得到π的相位差，选取半径为R1 = 82 nm和R2 = 121 nm的两个典型柱体，如图3(a)中的黑色虚线所示。结果表明，两柱体的π相位差恒定，透射系数分别高达0.987和0.982。

**Fig. 3.** (a) Curve of the additional phase shift and the transmission coefficient of a cylindrical dielectric antenna, when the radius $R$ of a cylinder varies from 50 to 150 nm. (b) and (c) Normalized electric fields $E_x$ in the $xz$-plane of the two cylinders with $R_1 = 82$ nm and $R_2 = 121$ nm, respectively.

0.987 and 0.982, respectively. Figures 3(b) and 3(c) show the normalized electric field distribution of two cylinders with radius of $R_1$ and $R_2$ in the $xz$-plane with $x$-pol light incident. Light is incident from the substrate direction and propagates along the $z$ axis. There is a phase difference of $\pi$ between the two electric fields when the light leaves these cylindrical antennas. We should also note that there is a sudden transmission coefficient drop occurring around $R = 134$ nm at 660 nm. It can mainly result from Fano resonance [36], which relates to both the radii $R$ of the nanopillar and the refractive index of material. Due to applying a relatively high aspect ratio (the ratio of height to width) nanopillar, it operates as a low-$Q$ FP cavity and accompanies a wavelength-dependent (with a specific particle size) transmittance dip. For a $TiO_2$-based nanostructure, the same effect has already been observed in several cases [37,38].

Simulation of a cylindrical antenna in the visible light band from 650 to 690 nm is carried out. For the DG shown in Fig. 2(a), when the $x$-pol light is incident normally, the simulation results show that the transmission phase difference of the two cylinders with different radii is always constant to $\pi$ [as shown in Fig. 4(a)], while maintaining a high transmission coefficient as high as 92% in the waveband from 650 to 690 nm [as shown in Fig. 4(b)]. It shows that our all-dielectric antenna is suitable for wide waveband application. The transmission spectrum slightly drops at some wavelengths, due to transmission loss, which is mainly caused by the reflection at the interface between the substrate and the cylindrical antenna [39]. We reduce the reflection loss and improve the transmission

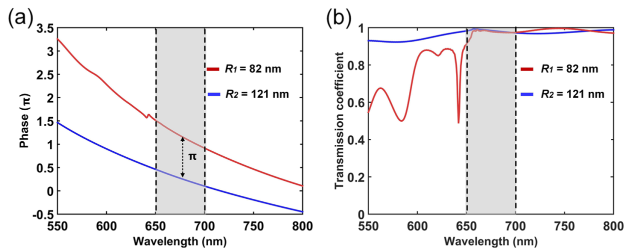


**Fig. 4.** (a) Transmission phase difference and (b) transmission coefficient of the cylindrical dielectric antenna with two radii of $R_1 = 82$ nm and $R_2 = 121$ nm form 550 to 800 nm with $x$-pol light incident. The red line indicates a dielectric antenna with radius $R_1 = 82$ nm; the blue line indicates a dielectric antenna with radius $R_2 = 121$ nm.

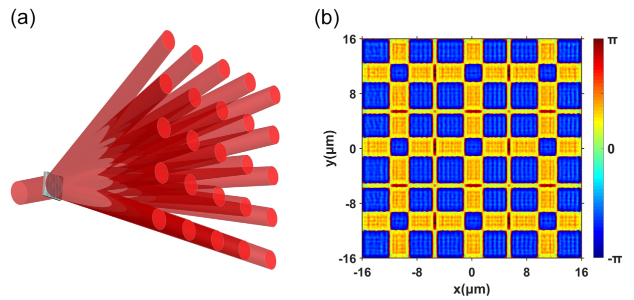


**Fig. 5.** (a) Schematic diagram of the light splitting of the 2D DG, which splits the incident beam into a 5 × 5 uniform spot array. (b) Electric field phase distribution of $E_x$ of the transmitted field in $xy$ plane when $z$ is 1.6 μm.

coefficient from 650 to 690 nm by allocating different materials for the cylindrical antenna and the substrate.

This DG as shown in Fig. 5(a) is capable of dividing the incident beam into a uniform 5×5 spot array with a diffraction angle of 20° × 20°. The two $TiO_2$ cylinders with different radii $R_1$ and $R_2$ are arranged on a silica substrate to provide a phase difference of $\pi$, and a period of the DG is 10.8 μm. In the actual simulation process, three periods of DGs in the $x$ and $y$ directions are arranged, respectively, with a total size of 32.4 μm × 32.4 μm, and the perfect matching layer (PML) in the $z$ direction. Figure 5(b) shows the phase distribution of the transmitted electric field $E_x$ of the DG. One can clearly distinguish the different divisions of the DG, and the electric field phase differences are approximately 0 or $\pi$, as we proposed. We obtain a 5 × 5 diffraction spot array. The DG has 25 diffraction orders in total, which is a superposition of five diffraction orders from −2 to 2 in the $x$ and $y$ directions, respectively. Since the 2D DG is a logical superposition of two identical 1D DGs, the distance between adjacent diffraction orders in the $x$ and $y$ directions of the diffraction spot array is all equal forming a 5 × 5 square spot array with uniform intensity.

## 3. RESULTS AND DISCUSSION

Based on the proposed DG, we conduct numerical simulation to analyze and evaluate the diffraction field generated by our DG from 650 to 690 nm. First, with an $x$-pol Laguerre–Gaussian beam at 660 nm incident on the DG, a 5 × 5 nearly uniform diffraction spot array is obtained, and the normalized light intensity distribution of it is shown in Fig. 6(a). In order to clearly characterize the uniformity of the spot array, the 3D light intensity distribution between the diffraction orders is shown in Fig. 6(e). Numerical calculation of the conversion efficiency can be given by Eq. (4), which is as high as 61.31%, and the contrast ratio can be calculated by Eq. (5), which reaches 0.3194. The diffraction angle is 20° × 20°, which can be adjusted by designing the grating constant. From Figs. 6(a) and 6(e), the intensity field is generally uniform with slight fluctuation, and the light spots located at the corner have relative lower intensity compared with central orders, mainly because of energy losses. The uniform intensity results from the high-order diffraction contribution, which are usually neglected in theoretical calculations based on the Dammann theory. Moreover, owing to the subwavelength structure with unit radius size along each direction less than half of the wavelength, high diffraction orders propagate in the evanescent mode and cannot reach the far field, which improves the signal-to-noise ratio of the output spot array to a certain high extent. Also, transmission loss caused by reflection is another reason for the nonuniform intensity of the spot array, which happens when the light transmits from the substrate to the cylindrical antenna array. The initial factors that reduce the contrast ratio is the intensity at (0,0) diffraction order, which is relatively weak compared with other central orders. However, this is a common effect, i.e., the so-called zero-order dark spot phenomenon, and can be further optimized and eliminated by symmetric coding. Excluding the zero-order intensity, the contrast ratio is as small as 0.254.

The structure of the cylinder is C4 symmetric and polarization-insensitive; thus, the DG is capable for light incident with different states of polarization (SoP). Figure 6(b) is the normalized light intensity distribution of the diffraction spot array with the $y$-pol Laguerre–Gaussian beam at 660 nm incident. Figure 6(f) is the 3D light intensity distribution at this moment. It can be seen that the distribution of the 5 × 5 square spot array is still uniform. The conversion efficiency reaches 61.06%, and the contrast ratio is 0.314, which proves the polarization-insensitive of our DG. Besides different LP incidences, we also choose SoP as left circularly polarized light (LCP) and right circularly polarized light (RCP) for simulation. The corresponding spot arrays are shown in Figs. 6(c) and 6(d), and the 3D light intensity distributions are shown in Figs. 6(g) and 6(h), respectively. The conversion efficiency is 61.22% and 60.79%, and the contrast ratio is 0.3247 and 0.3223, for LCP and RCP incident, respectively. The efficiency is still high ,and the intensity of spot array is uniform as well, which further proves that the proposed DG is polarization-insensitive. The conversion efficiency for each case is more than 60%, a little lower than that at the design stage, which is 83.5%, and the contrast ratio is higher than 0.053 in design. The designed conversion efficiency and contrast ratio are calculated on a standard phase-modulated DG. Our DG uses high-density cylindrical antennas to simulate the standard phase-modulated DG. Although the dielectric antenna has much lower ohmic loss compared with the metallic structure, it has slight energy decrease due to material absorption, reflection,

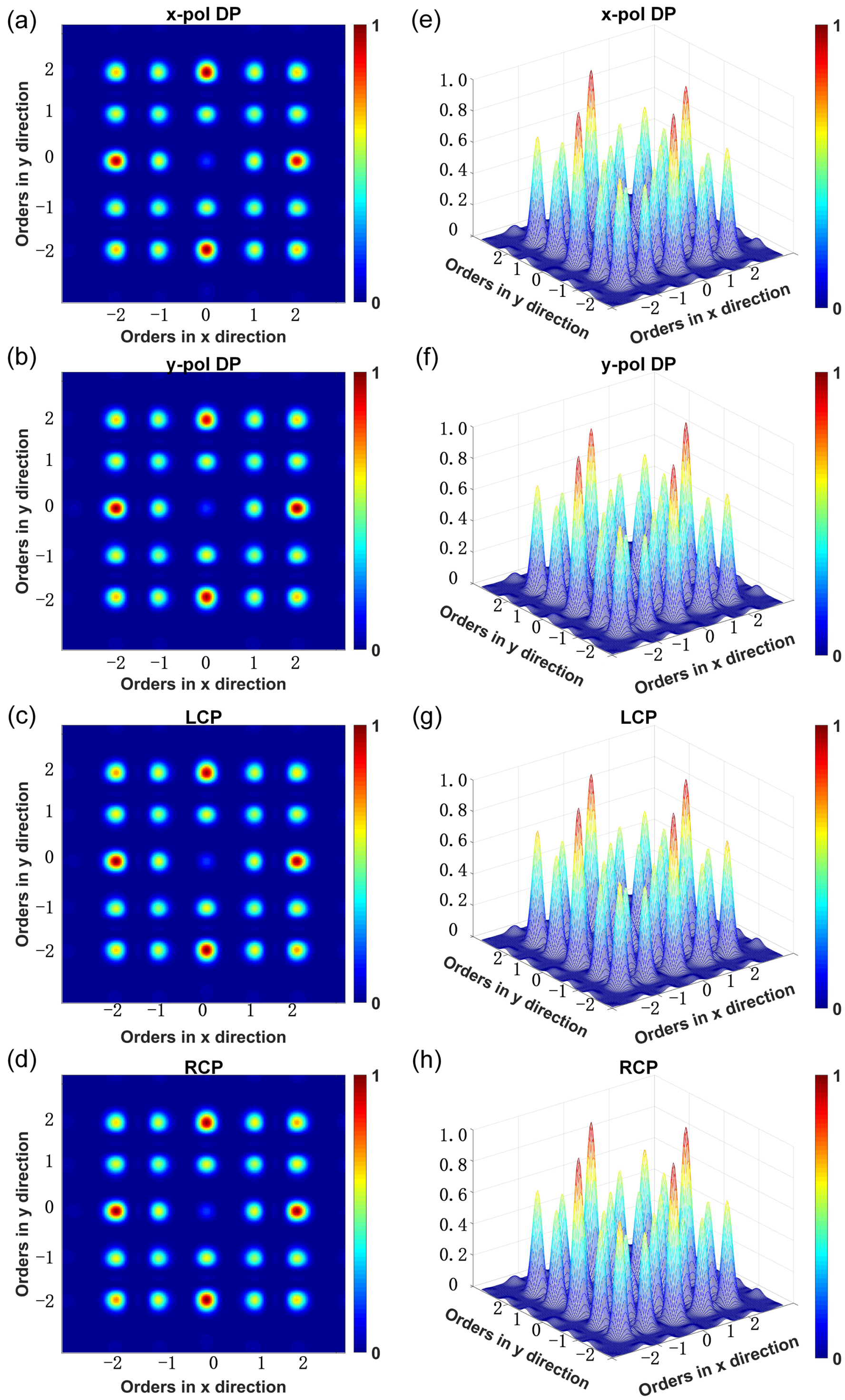


**Fig. 6.** (a)–(d) Normalized light intensity distribution of the diffraction spots when plane waves at 660 nm with four different polarization states are incident, respectively. (e)–(h) 3D normalized light intensity distribution. The incident light with four polarization states are $x$-pol light, $y$-pol light, LCP, and RCP.

and so on. Meanwhile, the near-field coupling between cylindrical dielectric antennas may also introduce unnecessary phase response and reduce the conversion efficiency of the DG.

Since the transmission phase difference of the two cylindrical antennas from 650 to 690 nm is almost always $\pi$, we use simulation to verify that the DG could work well in a certain wide waveband. From 650 and 690 nm, four typical wavelengths of $x$-pol light are chosen to be incident on the DG to obtain far-field distribution. We show the normalized light intensity distribution of the diffraction spots at 650, 670, 680, and 690 nm in Figs. 7(a)–7(d), and the corresponding 3D light intensity distributions are shown in Figs. 7(e)–7(h).

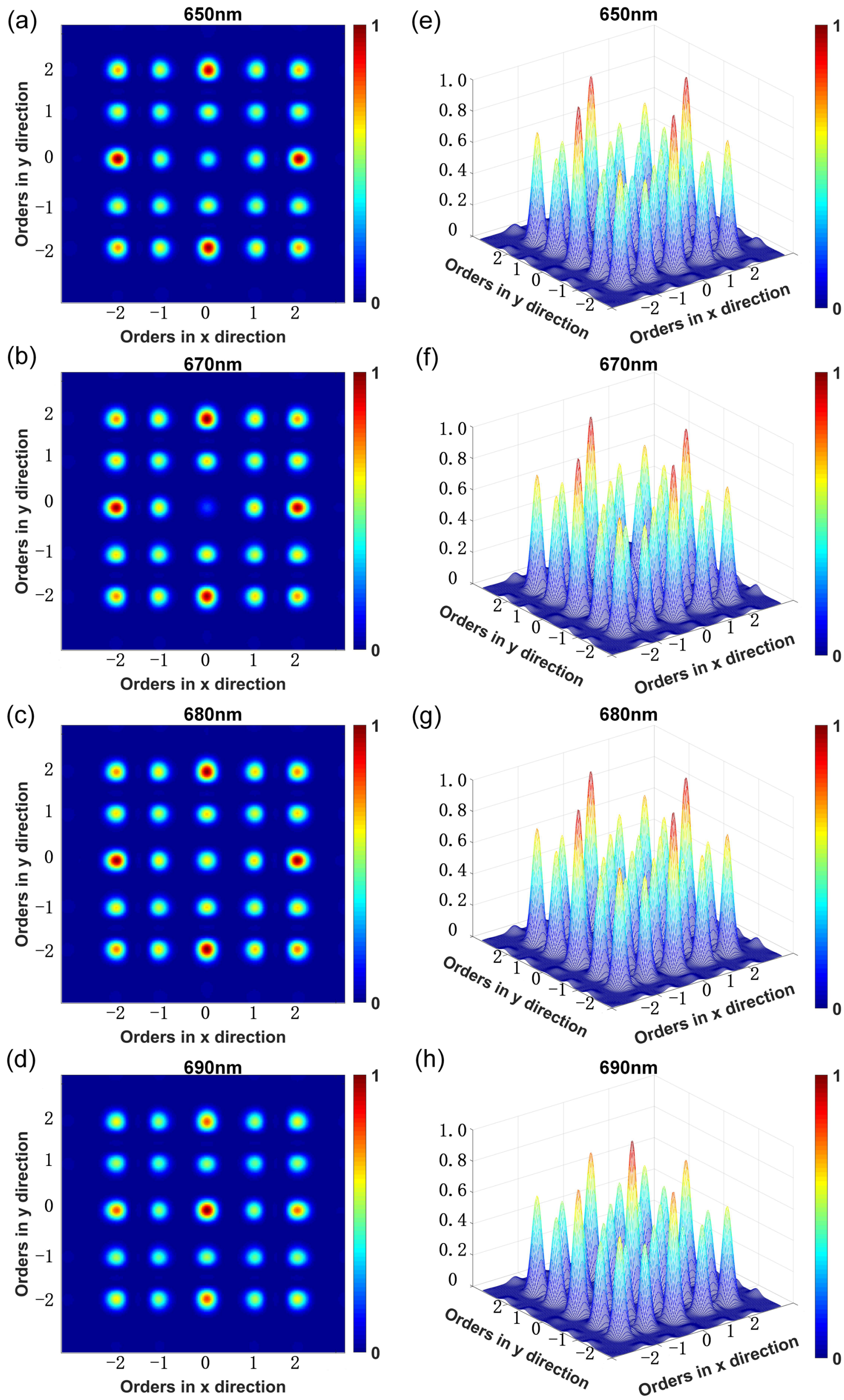


**Fig. 7.** (a)–(d) Normalized light intensity distribution of the diffraction spot array. (e)–(h) 3D normalized light intensity distribution in the incident of $x$-pol light at wavelengths of 650, 670, 680, and 690 nm.

The calculated conversion efficiencies are as high as 62.38%, 62.85%, 62.78%, and 64.35%; the contrast ratios are as small as 0.2836, 0.2853, 0.2268, and 0.2514 at 650, 670, 680, and 690 nm. It can be seen that our DG can obtain excellent beam-splitting effects at these wavelengths. The variation curve of the conversion efficiency and contrast ratio of the DG from 650 to 690 nm is shown in Fig. 8. For this waveband, it can be observed that the conversion efficiency does not change significantly, all above 62%, and the uniformity of the diffraction spot array is in good performance, all below 0.32 in the contrast ratio. The DG is not only polarization-insensitive but also works in a wide waveband, which expands its application range.

Manufacturing of normal cylindrical dielectric antennas can be realized by standard electron beam lithography [40,41]. For high-aspect-ratio nanopillar-based metasurfaces (approaching 20:1 in [42]), which applied a similar design as we proposed,

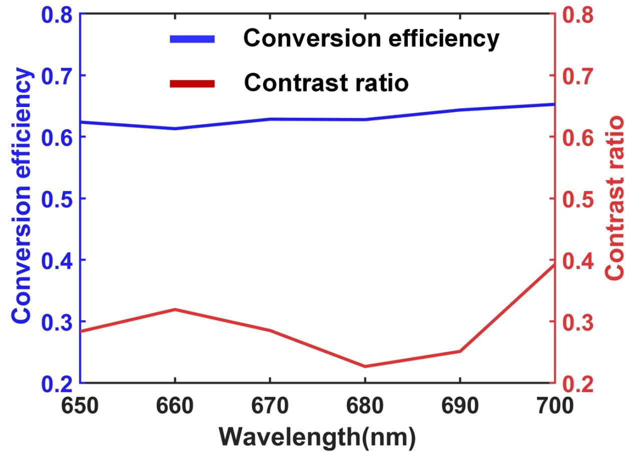


**Fig. 8.** Conversion efficiency (blue, $y$ axis on the left) and the contrast ratio (red, $y$ axis on the right) of the DG as a function of wavelength from 650 to 700 nm.

**Table 1. Comparison with Previous Works**

| Paper | Bandwidth | Conversion Efficiency | Contrast Ratio | Diffraction Angle |
|---|---|---|---|---|
| This work | 650–690 nm | >60% | <33% | $20^\circ \times 20^\circ$ |
| [13] | 1530–1565 nm | 50%–52% | 4.67% | $59^\circ \times 59^\circ$ |
| [14] | 1550 nm | 40.1% | 49% | $18^\circ \times 18^\circ$ |
| [15] | 780 nm | 57.2% | NA | NA |
| [16] | 633 nm | NA | 24.3% | $32^\circ \times 32^\circ$ |
| [17] | 1550 nm | 59.1% | 38.68% | $120^\circ \times 120^\circ$ |

its fabrication can employ the atomic layer deposition (ALD) method [43]. The metasurface structure consisting of an array of $TiO_2$ cylinders on a silica substrate is relatively simple, using only two different radii of cylinders to obtain different phase modulation in DG. In addition, the DGs based on cylindrical dielectric antennas shown here have higher robustness and are more tolerant against fabrication uncertainties due to their polarization-insensitive and wide waveband characteristics.

Table 1 lists a detailed comparison of this work with previous similar works on 2D all-dielectric DGs in terms of some pivotal factors. Although the all-dielectric DG is not the first time to be investigated, most of them work in the near-infrared, especially in the telecom waveband. Our DG is applied in a visible light wide waveband from 650 to 690 nm. In addition, ours has higher efficiency and better uniformity compared with previous work. Finally, compared with the circular polarization incident light required to be incident on the DG in some work, our DG is polarization-insensitive.

## 4. CONCLUSION

In summary, we propose a new DG based on the metasurface of an all-dielectric cylindrical antenna array. Using a $TiO_2$ nanopillar as the unit structure, the metasurface is able to control phase flexibly and efficiently shape the wavefront. Different phase shifts could be obtained by adjusting the radius of the cylindrical dielectric antenna while keeping the high transmission coefficient. Based on this principle, we design and comprehensively study a 2D DG with two sizes of $TiO_2$ cylinders on a silica substrate. The DG produces a $5 \times 5$ uniform diffraction spot array in the far field. In the wide operation waveband from 650 to 690 nm, the conversion efficiency can reach $\geq$60% and the contrast ratio is $\leq$0.33. All of its dielectric antennas are cylinders with C4 symmetry, which makes the DG polarization-insensitive. Our DG is only composed of two cylinders with different radii, which makes the actual manufacturing process easier. The design of our 2D DG is derived from the 1D DG, which is easy to design and optimize and can be further expanded according to actual work needs. The DG can be used in new laser technology and optical information transmission and processing.

**Disclosures.** The authors declare no conflicts of interest.

**Data availability.** Data underlying the results presented in this paper are not publicly available at this time but may be obtained from the authors upon reasonable request.

## REFERENCES

1. H. Dammann and K. Görtler, "High-efficiency in-line multiple imaging by means of multiple phase holograms," Opt. Commun. **3**, 312–315 (1971).
2. G. J. Swanson, "Binary optics technology: the theory and design of multi-level diffractive optical elements," Technical Report (Massachusetts Institute of Technology, Lexington Lincoln Laboratory, 1989).
3. R. L. Morrison, S. L. Walker, and T. J. Cloonan, "Beam array generation and holographic interconnections in a free-space optical switching network," Appl. Opt. **32**, 2512–2518 (1993).
4. C. Zhou and L. Liu, "Numerical study of Dammann array illuminators," Appl. Opt. **34**, 5961–5969 (1995).
5. E. Dai, C. Zhou, and G. Li, "Dammann SHG-FROG for characterization of the ultrashort optical pulses," Opt. Express **13**, 6145–6152 (2005).
6. J. Li, Y. Yao, J. Yu, K. Xia, and C. Zhou, "Efficient vortex laser with annular pumping formed by circle Dammann grating," IEEE Photon. Technol. Lett. **28**, 473–476 (2015).
7. K. Liu, C. Zhou, S. Wei, S. Wang, X. Fan, and J. Ma, "Optimized stereo matching in binocular three-dimensional measurement system using structured light," Appl. Opt. **53**, 6083–6090 (2014).
8. J. Yu, C. Zhou, W. Jia, A. Hu, S. Wang, and J. Ma, "Circular Dammann grating under high numerical aperture focusing," Appl. Opt. **51**, 994–999 (2012).
9. J. Yu, C. Zhou, W. Jia, A. Hu, W. Cao, J. Wu, and S. Wang, "Three-dimensional Dammann vortex array with tunable topological charge," Appl. Opt. **51**, 2485–2490 (2012).
10. J. Yu, C. Zhou, W. Jia, J. Ma, A. Hu, J. Wu, and S. Wang, "Distorted Dammann grating," Opt. Lett. **38**, 474–476 (2013).
11. H. Wang, H. Wang, W. Zhang, and J. K. Yang, "Toward near-perfect diffractive optical elements via nanoscale 3D printing," ACS Nano **14**, 10452–10461 (2020).
12. Z.-N. Yuan, Z.-B. Sun, H.-S. Kwok, and A. K. Srivastava, "Fast lidar systems based on ferroelectric liquid crystal Dammann grating," Liq. Cryst. **48**, 1402–1416 (2021).
13. Z. Li, G. Zheng, S. Li, Q. Deng, J. Zhao, and Y. Ai, "All-silicon nanorod-based Dammann gratings," Opt. Lett. **40**, 4285–4288 (2015). 13-18 超表面用于达曼光栅设计
14. S. Yang, C. Li, T. Liu, H. Da, R. Feng, D. Tang, F. Sun, and W. Ding, "Simple and polarization-independent Dammann grating based on all-dielectric nanorod array," J. Opt. **19**, 095103 (2017).
15. L. Huang, S. Xu, B. Reineke, T. Li, and T. Zentgraf, "Volumetric generation of optical vortices with metasurfaces," ACS Photon. **4**, 338–346 (2017).
16. K. Chen, Y. Wang, T. He, Y. Cui, J. Tao, Z. Li, and G. Zheng, "Metasurface fan-out diffractive optical elements," J. Appl. Opt. **40**, 306–310 (2019).
17. Y. Ni, S. Chen, Y. Wang, Q. Tan, S. Xiao, and Y. Yang, "Metasurface for structured light projection over 120° field of view," Nano Lett. **20**, 6719–6724 (2020).

18. Z. Ye, W. Liu, P. Sun, G. Jin, J. Li, Y. Xie, C. Zhou, and W. Jia, “Equilateral triangle hexagonal array by crossing two one-dimensional Dammann gratings with 60°,” Microw. Opt. Technol. Lett. **63**, 2297–2302 (2021).
19. H. Zhang, Z. Zhang, X. Song, R. Zhao, D. Jia, and T. Liu, “Tunable multi-wavelength optofluidic Dammann grating with beam splitting property,” Opt. Express **29**, 33414–33423 (2021).
20. L. Guo and J. Wang, “A high-diffraction-efficiency subwavelength silica Dammann grating,” Optik **157**, 319–325 (2018).
21. N. Yu, P. Genevet, M. A. Kats, F. Aieta, J.-P. Tetienne, F. Capasso, and Z. Gaburro, “Light propagation with phase discontinuities: generalized laws of reflection and refraction,” Science **334**, 333–337 (2011).
22. A. Arbabi, Y. Horie, M. Bagheri, and A. Faraon, “Dielectric metasurfaces for complete control of phase and polarization with subwavelength spatial resolution and high transmission,” Nat. Nanotechnol. **10**, 937–943 (2015).
23. A. I. Kuznetsov, A. E. Miroshnichenko, M. L. Brongersma, Y. S. Kivshar, and B. Luk’yanchuk, “Optically resonant dielectric nanostructures,” Science **354**, aag2472 (2016).
24. Q. Zhao, J. Zhou, F. Zhang, and D. Lippens, “Mie resonance-based dielectric metamaterials,” Mater. Today **12**(12), 60–69 (2009).
实现可见光波段激光光束分裂的超表面
25. Z. Li, E. Palacios, S. Butun, and K. Aydin, “Visible-frequency metasurfaces for broadband anomalous reflection and high-efficiency spectrum splitting,” Nano Lett. **15**, 1615–1621 (2015).
26. J. Jin, M. Pu, Y. Wang, X. Li, X. Ma, J. Luo, Z. Zhao, P. Gao, and X. Luo, “Multi-channel vortex beam generation by simultaneous amplitude and phase modulation with two-dimensional metamaterial,” Adv. Mater. Technol. **2**, 1600201 (2017).
27. J. Wang, Q. Jiang, and D. Han, “Multi-channel beam splitters based on gradient metasurfaces,” Results Phys. **24**, 104084 (2021).
28. F. Ding, R. Deshpande, C. Meng, and S. I. Bozhevolnyi, “Metasurface-enabled broadband beam splitters integrated with quarter-wave plate functionality,” Nanoscale **12**, 14106–14111 (2020).
29. F. Presutti and F. Monticone, “Focusing on bandwidth: achromatic metalens limits,” Optica **7**, 624–631 (2020).
30. R. L. Morrison, “Symmetries that simplify the design of spot array phase gratings,” J. Opt. Soc. Am. A **9**, 464–471 (1992).
31. I. Moreno, J. A. Davis, D. M. Cottrell, N. Zhang, and X.-C. Yuan, “Encoding generalized phase functions on Dammann gratings,” Opt. Lett. **35**, 1536–1538 (2010).
32. J. N. Mait, “Design of binary-phase and multiphase Fourier gratings for array generation,” J. Opt. Soc. Am. A **7**, 1514–1528 (1990).
33. S. D. Mellin, *Design and Analysis of Finite-Aperture Diffractive Optical Elements* (The University of Alabama in Huntsville, 2001).
34. Y. Yang, W. Wang, P. Moitra, I. I. Kravchenko, D. P. Briggs, and J. Valentine, “Dielectric meta-reflect array for broadband linear polarization conversion and optical vortex generation,” Nano Lett. **14**, 1394–1399 (2014).
35. S. J. Byrnes, A. Lenef, F. Aieta, and F. Capasso, “Designing large, high-efficiency, high-numerical-aperture, transmissive meta-lenses for visible light,” Opt. Express **24**, 5110–5124 (2016).
36. U. Fano, “Effects of configuration interaction on intensities and phase shifts,” Phys. Rev. **124**, 1866–1878 (1961).
37. J. T. Choy, J. D. Bradley, P. B. Deotare, I. B. Burgess, C. C. Evans, E. Mazur, and M. Lončar, “Integrated $TiO_2$ resonators for visible photonics,” Opt. Lett. **37**, 539–541 (2012).
38. Y. Huang, G. Pandraud, and P. M. Sarro, “Reflectance-based two-dimensional $TiO_2$ photonic crystal liquid sensors,” Opt. Lett. **37**, 3162–3164 (2012).
39. D. Lin, P. Fan, E. Hasman, and M. L. Brongersma, “Dielectric gradient metasurface optical elements,” Science **345**, 298–302 (2014).
40. J. Kyoung, E. Y. Jang, M. D. Lima, H.-R. Park, R. O. Robles, X. Lepró, Y. H. Kim, R. H. Baughman, and D.-S. Kim, “A reel-wound carbon nanotube polarizer for terahertz frequencies,” Nano Lett. **11**, 4227–4231 (2011).
41. G. Yoon, K. Kim, D. Huh, H. Lee, and J. Rho, “Single-step manufacturing of hierarchical dielectric metalens in the visible,” Nat. Commun. **11**, 2268 (2020).
42. E. Schonbrun, K. Seo, and K. B. Crozier, “Reconfigurable imaging systems using elliptical nanowires,” Nano Lett. **11**, 4299–4303 (2011).
43. R. C. Devlin, M. Khorasaninejad, W. T. Chen, J. Oh, and F. Capasso, “Broadband high-efficiency dielectric metasurfaces for the visible spectrum,” Proc. Natl. Acad. Sci. USA **113**, 10473–10478 (2016).